Numerical simulation of phase separation coupled with crystallization

Douglas Zhou,[1] An-Chang Shi,[2,a)] and Pingwen Zhang[3,b)]
[1]*School of Mathematical Sciences, Peking University, Beijing 100871, People's Republic of China*
[2]*Department of Physics and Astronomy, McMaster University, Hamilton, Ontario L8S 4M1, Canada*
[3]*Laboratory of Mathematics and Applied Mathematics and School of Mathematical Sciences, Peking University, Beijing 100871, People's Republic of China*

(Received 31 December 2007; accepted 9 September 2008; published online 15 October 2008)

The kinetics of liquid-liquid phase separation and polymer crystallization observed in double-quench experiments with blends of poly(ethylene-co-hexene) and poly(ethylene-co-butene) are studied using time-dependent Ginzburg–Landau Model. Numerical simulations demonstrate that our model can successfully reproduce three experimental phenomena: The decrease in number and size of crystallized spherulites with increasing time in phase separation, the preponderance of nuclei near the domain interface, and the subphase separation and subcrystallization occurring when the second quench is very deep. Moreover, the simulations are consistent with the recently proposed mechanism of "phase separation fluctuation assisted nucleation" in the crystallization process.
 [DOI: 10.1063/1.2992530]

I. INTRODUCTION

Phase separation has attracted a great deal of attention for several decades.[1–3] In particular, phase diagrams have been determined both theoretically and experimentally,[4–6] and dynamic behaviors, especially the growth of domain size, have been studied extensively.[7–10] Meanwhile, the kinetics of crystallization has also been extensively studied.[11,12] Much work has been carried out experimentally and with Monte Carlo simulations.[13–19] Interactions between phase separation and crystallization processes are usually present in a blend system, in which one component is crystalline and another component is amorphous. It is very interesting to study the coupling of these two nonequilibrium phenomena because they can produce some new structures and dynamics which are important from both scientific and industrial viewpoints. Several studies have been performed on static morphological structures. Nevertheless, most experiments are concentrated on either single quenching or multiple quenching starting from the early stages of phase separation. The two-step quench experiment starting from late stages of phase separation, especially when the second quench involves crystallization, remains less explored. In another words, the interplay between these two nonequilibrium phenomena has been largely neglected due to its complexity. Only a few investigations have been carried out to study this complex interaction.[20–28] Therefore, further investigations are desirable to obtain an overall understanding of the dynamic relationships between coexisting liquid-liquid phase separation (LLPS) and crystallization.

Recently Han and co-workers studied the interplay between LLPS and crystallization in blends of statistical copolymers, poly(ethylene-co-hexene) (PEH) and poly(ethylene-co-butene) (PEB), using multiple quenching schemes.[29–33] In contrast to earlier work, they have paid special attentions to the kinetic coupling between phase separation and crystallization. The pattern formation of LLPS and crystallized structures were observed by using phase-contrast bright-field optical microscopy and polarized light microscopy, respectively. Further investigation of the changes in crystallization kinetics were performed using differential scanning calorimetry and atomic force microscopy (AFM). Their various experiments demonstrate changes in nucleation rate and crystallinity. To explain this change in crystallization kinetics, they proposed a mechanism of heterogeneous nucleation assisted by the liquid-liquid spinodal decomposition, which is presented as phase separation fluctuation assisted nucleation. The idea that the nucleation rate could be assisted by the concentration fluctuations due to spontaneous spinodal LLPS is quite different from the crystallization process in a one component system.

Inspired by these recent experiments, we present a phenomenological model to describe the interplay between LLPS and crystallization. Specifically, time-dependent Ginzburg–Landau (TDGL) equations,[34–36] have been developed to study the spatiotemporal evolution of a conserved compositional order parameter and a nonconserved crystalline order parameter (model C). In the literature, polymer crystallization is usually associated with the Hoffman–Lauritzen (HL) theory. The HL theory is capable of describing many features of polymer crystal growth processes.[37–39] However, the HL theory deals with the growth of large crystals via nucleation at the crystal surface. Furthermore, the original HL kinetic theory does not contain a description of the spatial diffusion of the interface for crystal growth. On the other hand, the Ginzburg–Landau theory has the capability of describing spatial and temporal variations. For example, a number of studies using phase field model derived from coupled TGDL model C have been successfully applied to the crystal growth in metal alloys[20] and eutectic crystal growth,[36] as well as the elucidation of rhythmic growth of

a)Electronic mail: shi@mcmaster.ca.
b)Electronic mail: pzhang@pku.edu.cn. Tel.: +86-10-6275-9851. FAX: +86-10-6276-7146.

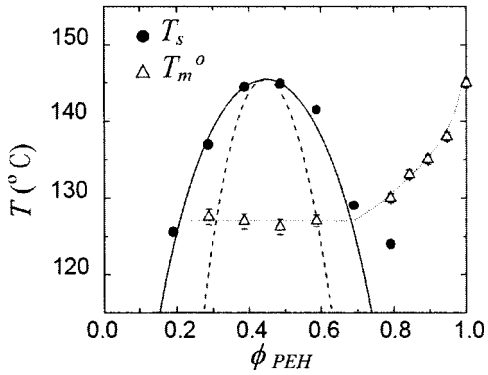

FIG. 1. Phase diagram of PEB/PEH blends taken from Ref. 29. The symbols (filled circles) correspond to experimental data points of the binodal temperature (T_s) and the solid line is the fit of the Flory–Huggins theory. The additional symbols (open triangles) display the equilibrium melting points of blends observed in the experiments. The equilibrium melting temperature curve is obtained by the Hoffman–Weeks extrapolation method.

concentric and spiral spherulites in a binary polymer blend containing a crystalline polymer as one component.[21] Following the same philosophy, a classical Landau-type double-well potential is used to represent the free energy of the phase separation and the crystallization.[20,40] In addition, we construct a coupling free energy which reflects the kinetic intertwining of LLPS and crystallization, especially the mechanism of "phase separation fluctuation assisted nucleation." Numerical results demonstrate that our model can reproduce almost all of the dynamic features observed in the experiments.

After summarizing the salient experimental results supporting the newly proposed mechanism, we will interpret these results and present our dynamic models. We also obtain the phase diagram through solving the TDGL equations self-consistently. This method has been presented recently and has been successful in determining the phase diagram of both crystalline-amorphous and crystalline-crystalline polymer blends.[4–6,41–44] Moreover we will describe our simulation and show how it is consistent with the experimental results on the changes in crystallization kinetics and with the new mechanism proposed to explain those results.

II. EXPERIMENTAL OBSERVATION

The interplay between LLPS and crystallization in a binary blend of crystallizable PEH and noncrystallizable PEB has been examined using multiple quenching schemes.[31–33] These polymer systems are quite suitable for studying the kinetic coupling between LLPS and crystallization because the phase separation process takes place very slowly due to the similarity in monomer structures between PEH and PEB. The phase diagram of PEH/PEB blends (Fig. 1) (Ref. 29) exhibits an upper critical solution temperature, with a critical temperature of 146 °C at a critical composition of $\phi_{\mathrm{PEH}}=0.44$. The melting temperature of blends in the phase separation region is almost a constant of 127 °C.

The pattern formation under various conditions has been examined by optical microscopy, AFM, and differential scanning calorimetry. The phase contrast optical microscopy shows interconnected bicontinuous structures for the first temperature quench,[31–33] which are characteristics of spinodal decomposition. After a second quench to a temperature below the melting point, an overwhelming change in crystallization kinetics has been clearly observed, which is quite different from the crystallization of one component system.[16–18,45] The main experimental observations are summarized as follows:

- The number and size of crystallized spherulite decrease with increasing time of LLPS after the first temperature quench. This implies that the concentration fluctuation due to early stage of phase separation can give rise to nuclei for crystallization.[31,32]
- Most of the nuclei are located near the interface of the phase-separated domains; only a few are in the PEH rich domains.[31,32]
- Subphase separation and subcrystallization occur if the second quench is very deep (to room temperature). This implies that small secondary domains of polymer blends and crystallized spherulites appear in the larger primary domains which are formed during LLPS.[33]

III. MODEL DESCRIPTION

We first give some explanations of the experimental phenomena, which will also shed light to dynamic modeling. The decrease in number and size of crystallized spherulite associated with time in LLPS and the predominance of nuclei near the domain interface can be explained by the fact that the interfacial region of a phase separating system is favorable to the crystallization process (the appearance of nuclei and the number of nuclei). This is because the longer the time spent in LLPS after the first quench, the sharper the interface and the smaller the interfacial region becomes, rendering it less probable that LLPS assisted nucleation will occur. The same intrinsic mechanism underlies the third phenomenon, the subphase separation and subcrystallization occurring when the second quench is very deep. Even if LLPS is complete at the end of the first quench, the concentration fluctuation will still be large when the second quench is very deep. That is, the concentrations of both PEH-rich and PEB-rich domains formed in LLPS by the first quench will still fall into a new spinodal decomposition region in the phase diagram by the second deep quench. Moreover the correlation length of fluctuation after the second deep quench will be much smaller compared to that of the first quench. This causes the occurrence of a subphase separation process.

The dynamics of phase separation and crystallization are described using a TDGL theory. The TDGL model equations are basically two nonlinear diffusion equations in which a conserved compositional order parameter (ϕ) is coupled with a nonconserved orientational crystalline order parameter (ψ), namely,

$$\frac{\partial \phi}{\partial t} = \nabla\left(M_\phi \nabla \frac{\delta F(\phi,\psi)}{\delta \phi}\right) + \eta_\phi,$$

$$\frac{\partial \psi}{\partial t} = -M_\psi \frac{\delta F(\phi,\psi)}{\delta \psi} + \eta_\psi, \tag{1}$$

where M_ϕ and M_ψ are Onsager coefficients. They may depend on both the molecular weights and the order parameters. The last terms (η_ϕ and η_ϕ) in the above equation are thermal random forces which satisfy the fluctuation dissipation relations,

$$\eta_\phi(r_1,t_1)\,\eta_\phi(r_2,t_2) = -2M_\phi \nabla^2 \delta(r_1 - r_2)\,\delta(t_1 - t_2),$$

$$\eta_\psi(r_1,t_1)\,\eta_\psi(r_2,t_2) = 2M_\psi \delta(r_1 - r_2)\,\delta(t_1 - t_2).$$

The total free energy functional $F(\phi,\psi)$ is assumed to be given by

$$F(\phi,\psi) = \int \left[f_{\text{bulk}}(\phi,\psi) + \frac{\varepsilon_1}{2}(\nabla\phi)^2 + \frac{\varepsilon_2}{2}(\nabla\psi)^2 \right] dr,$$

where

$$f_{\text{bulk}}(\phi,\psi) = f_{\text{ps}}(\phi) + f_{\text{crys}}(\psi) + f_{\text{coup}}(\phi,\psi). \tag{2}$$

Here $F(\phi,\psi)$ consists of two parts, one is the bulk free energy and the other is interfacial free energy. The bulk free energy f_{bulk} contains the compositional ordering for phase separation, the orientational crystal ordering for crystallization, and the coupling of interaction between LLPS and crystallization. The interfacial free energy just contains the gradients jump in the interface of different regions. Phase separation is controlled by concentration fluctuation and the decrease in bulk energy in the early stage, which is also the stage when crystallization occurs in experiments. In the later stage, phase separation is controlled by diffusion and coarsening, and the decrease in interfacial free energy when no crystallization process takes place.

The compositional free energy (f_{ps}) is expressed in terms of Landau-type double-well potential[20,40]

$$f_{\text{ps}}(\phi) = w_1\left(\frac{r[T]}{2}\phi^2 + \frac{s}{3}\phi^3 + \frac{1}{4}\phi^4\right), \tag{3}$$

where w_1 is the weight factor of phase separation energy and s is a parameter which brings asymmetry to the system. The effective interaction parameter $r[T]$ increases with temperature T and is expressed as

$$r[T] = aT + b,$$

where a and b are undetermined parameters. The spinodal line of phase separation is determined by $f''_{\text{ps}}(\phi)=0$, namely,

$$\phi_1 = -\frac{s}{3} - \frac{\sqrt{s^2 - 3aT - 3b}}{3},$$

$$\phi_2 = -\frac{s}{3} + \frac{\sqrt{s^2 - 3aT - 3b}}{3}. \tag{4}$$

Therefore the sign of $(s^2 - 3aT - 3b)$ determines whether the potential has a single-well or a double-well structure.

The orientational crystalline free energy (f_{crys}) is described as follows:[20,40]

$$f_{\text{crys}}(\psi) = w_2\left(\int_0^\psi x(x-1)\left(x - \frac{1}{2} - \theta[T]\right)dx\right),$$

where w_2 is the weight factor of crystallization energy. This crystal phase order parameter may be defined as the ratio of the lamellar thickness and usually represents the one-dimensional crystallinity.[46,47] The monotonic increasing function of temperature T, $\theta[T]$, is expressed as

$$\theta[T] = \frac{1}{\pi}\arctan(T - T_m),$$

where T_m is the melting temperature. It is easy to verify that the energy f_{crys} has local minima at $\psi=0$ (amorphous state) and $\psi=1$ (crystalline state), and a local maximum at $\psi=\frac{1}{2} + \theta[T]$. The sign of $\theta[T]$ determines which state is the more stable global minimum.

The coupling free energy is the most important part of the model because it reflects the competition between these two nonequilibrium phenomena. Theoretically, it should be represented as a polynomial of the order parameters in order to be consistent with the forms of the compositional and crystal free energy. In our model we choose to express the coupling term as

$$f_{\text{coup}}(\phi,\psi) = w_3\psi(\phi - C_1[T])(\phi - C_2[T]),$$

where w_3 is the weight factor of the coupling energy and $C_1[T]$ and $C_2[T]$ correspond to the spinodal points in Eq. (4). The current form of this term is based on our understanding of the physical mechanism of fluctuation-induced nucleation. From a thermodynamic perspective, the equilibrium state should be the global minimum of the total free energy. When the composition of PEH in the phase is in the spinodal region ($C_1[T] < \phi < C_2[T]$) and the temperature is below the melting point in the phase diagram, the crystalline state will be more stable than the amorphous state since it corresponds to the lower energy for both the coupling part (f_{coup}) and the crystal ordering part (f_{crys}). That is, crystallization process will proceed much more easily because the energy barrier is reduced in the spinodal decomposition region. This is the mechanism of phase separation fluctuation assisted nucleation proposed by NIST and CAS groups.[31–33] Our numerical results indicate that our choice for the coupling part indeed reproduces the experimental observations.

It should be pointed out that the bulk terms given above for the free energy are not unique. It is possible to use other forms of the free energy for the bulk behavior. For example, polymer phase separation can also be described by the Flory–Huggins free energy. In fact, any free energy model with the essential properties can be used for studying generic features of the system. In all models, the parameters in the bulk free energy should be determined by the bulk phase behavior.

TABLE I. Equilibrium concentrations of phase separation in different temperatures taken from Ref. 31. Here * represents missing data.

T (°C)	123	125	128	138	142	145	146
ϕ_1^*	*	0.2	*	0.3	*	0.4	0.44
ϕ_2^*	0.8	*	0.7	*	0.6	0.54	0.44

IV. NUMERICAL SIMULATIONS

A. Phase diagram

We now try to determine the phase diagram of the system. A thermodynamically self-consistent theory has been developed for determination of phase diagrams of polymer solutions as well as polymer blends.[41–44] Following the same philosophy, we first minimize the total free energy density of mixing with respect to the crystal order parameter (ψ). This is the same as determining the roots at $\partial f/\partial\psi=0$, which can be solved on either the steepest descent algorithm[43] or analytical expression in our case,

$$\psi=-\frac{R}{3}+\sqrt[3]{-\frac{Q}{2}+\sqrt{D}}+\sqrt[3]{-\frac{Q}{2}-\sqrt{D}},$$

$$\psi=-\frac{R}{3}+\sqrt[3]{-\frac{Q}{2}+\sqrt{D}}\omega+\sqrt[3]{-\frac{Q}{2}-\sqrt{D}}\omega^2, \tag{5}$$

$$\psi=-\frac{R}{3}+\sqrt[3]{-\frac{Q}{2}+\sqrt{D}}\omega^2+\sqrt[3]{-\frac{Q}{2}-\sqrt{D}}\omega,$$

where $R=-3/2-\theta[T]$, $Q=2/27*R^3-R/3*(1/2+\theta[T])+w_3/w_2*(\phi-C_1[T])*(\phi-C_2[T])$, $D=Q^2/4+P^3/27$ and $P=1/2+\phi[T]-R^2/3$. ω is the cubic root of unit circle. Of course only two solutions in Eq. (5) are reasonable according to the global minimization satisfying $\partial^2 f/\partial\psi^2>0$. Subsequently the chemical potentials are calculated through minimization with respect to the compositional order parameter (ϕ), and the coexistence curves are determined with the aid of the double tangent construction[4–6]

$$f'_{\text{bulk}}(\phi_1^*,\psi(\phi_1^*))=f'_{\text{bulk}}(\phi_2^*,\psi(\phi_2^*))=\frac{f_{\text{bulk}}(\phi_2^*,\psi(\phi_2^*))-f_{\text{bulk}}(\phi_1^*,\psi(\phi_1^*))}{\phi_2^*-\phi_1^*}, \tag{6}$$

where $\psi(\phi)$ means that the crystal order parameter (ψ) is a function of the compositional order parameter (ϕ), which is chosen in Eq. (5) as the global minimum of the free energy density $[f_{\text{bulk}}(\phi,\psi)]$.

In order to assure that (ϕ) stays within the interval [0,1], where it represents the concentration exactly, we add some constant and linear terms of the compositional order parameter (ϕ) to the expression of free energy given in Eq. (3),

$$\tilde{\phi}_1^*=\frac{\phi_1^*+c}{d},\quad \tilde{\phi}_2^*=\frac{\phi_2^*+c}{d},$$

where c and d are undetermined parameters. The experimental data points of the equilibrium concentrations with different temperatures are shown in Table I.

TABLE II. Melting temperatures of crystallization for different concentrations.

ϕ_0	0.3	0.4	0.5	0.6	0.8	0.85	0.9	0.95	1.0
T_m (°C)	127.5	127	126.5	127	130	133	135	138.5	144

The melting temperature is determined by $\theta[T]=0$. Experimental data of the equilibrium melting temperatures for different initial concentrations are shown in Table II. We use the sectional interpolation method to obtain the melting temperature (T_m). That is, inside the phase separation region, T_m is chosen as a zero-order polynomial

$$T_m=e_1,$$

while outside the phase separation region, T_m is chosen as a third-order polynomial

$$T_m=a_1+b_1\psi+c_1\psi^2+d_1\psi^3,$$

where a_1, b_1, c_1, d_1, and e_1 are the parameters. All the coefficients in the model are determined by means of a least squares fitting method

$$a=0.25,\quad b=-36,\quad s=-1.32,\quad c=3.3,\quad d=8,$$

$$a_1=126.8,\quad b_1=26.6,\quad c_1=-98.8,\quad d_1=88.7,\quad e_1=127,$$

$$w_1=0.8,\quad w_2=80,\quad w_3=0.4.$$

Therefore we obtain a phase diagram of the binary system shown in Fig. 2.

B. Dynamics

Simulations are carried out in two dimension for the models presented above. We use a forward Euler method in time and a finite volume method in space to discretize the

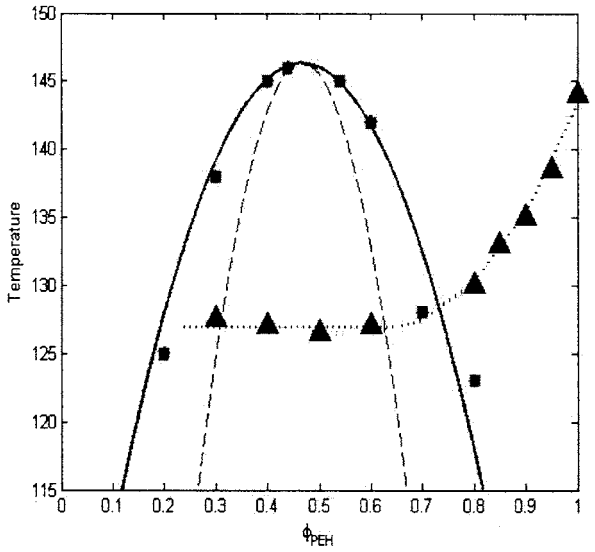

FIG. 2. Phase diagram of PEB/PEH blends. The squares correspond to experimental data points of the binodal temperature and the solid line is the fit of the Landau-type double-well energy. The triangles represent the equilibrium melting points obtained in experiments. The equilibrium melting temperature curve is obtained by sectional interpolation method.

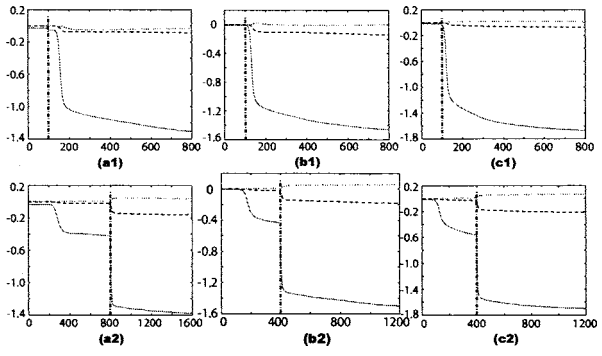

FIG. 3. Time evolution of the bulk phase separation energy (f_{ps}) (solid line), the bulk crystallization energy (f_{crys}) (dotted line), and the bulk coupling energy (f_{coup}) (dashed line) with data points recorded every 50 time steps, the second temperature-quench time is recorded by the dash dot line. The initial concentration (ϕ_0) and the second temperature-quench time (t^*) are (a1) $\phi_0=0.35$, $t^*=25$, (a2) $\phi_0=0.35$, $t^*=200$, (b1) $\phi_0=0.4$, $t^*=25$, (b2) $\phi_0=0.4$, $t^*=100$, (c1) $\phi_0=0.45$, $t^*=25$, (c2) $\phi_0=0.45$, and $t^*=100$.

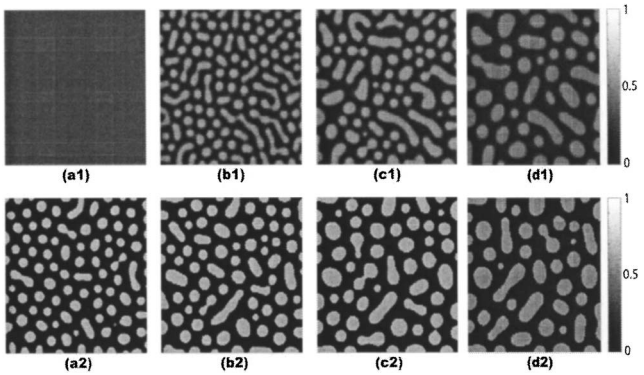

FIG. 4. Time evolution of compositional order parameter (ϕ) with PEH/PEB=40/60 and two different quench times (t^*) for upper row images (a1)–(d1) and lower row images (a2)–(d2). (a1) LLPS at 130 °C for $t=25$, then quenched to 121 °C for $t=0$, (b1) $t=25$, (c1) $t=75$, and (d1) $t=175$. (a2) LLPS at 130 °C for $t=100$, then quenched to 121 °C for $t=0$, (b2) $t=50$, (c2) $t=125$, and (d2) $t=200$.

equations. The grid size is set at $\Delta x=\Delta y=0.5$ and the system size is $N_x=N_y=128$. The time step is chosen as $\Delta t=0.005$. We use no-flux boundary conditions, namely,

$$\frac{\partial \phi}{\partial n}=0, \quad \frac{\partial \mu}{\partial n}=0, \quad \frac{\partial \psi}{\partial n}=0, \tag{7}$$

where μ is the chemical potential. The Onsager coefficients are chosen as $M_\phi=0.1$ and $M_\psi=0.1$ and the interfacial gradient parameters are chosen as $\varepsilon_1=1.0$ and $\varepsilon_2=0.2$. The simulated blend system under different initial concentrations undergoing LLPS at 130 °C for different times is then quenched to 121 °C for crystallization.

Figure 3 shows time evolution of the individual parts in the bulk free energy. We see that the binary system under all the initial concentrations stays in the immiscible two phase region in the phase diagram. Therefore, phase separation occurs via spinodal decomposition. In the early stage, the phase separation process is controlled by concentration fluctuations and the decrease in the bulk energy. In the later stage, however, phase separation process is controlled by diffusion and coarsening, and the decrease in interfacial free energy. As a result, the variation of the bulk phase separation energy (f_{ps}) indicates which stage the second temperature-quench time corresponds to. It is clear that the second temperature-quench time (dash dot line in Fig. 3) shown in the upper row image in Fig. 3 corresponds to the early stage of LLPS by the first temperature quench, while that in the lower row image in Fig. 3 corresponds to the later stage of LLPS.

Figure 4 shows time evolution of the compositional order parameter with the PEH/PEB=40/60 and different quench times t^*. The upper row of image [from (a1) to (d1)] corresponds to the blend system undergoing LLPS at 130 °C for $t=25$ and then isothermally crystallized at 121 °C for $t=0$, $t=25$, $t=75$, and $t=175$, respectively. The lower row of image [from (a2) to (d2)] corresponds to the blend system undergoing LLPS at 130 °C for $t=100$ and then isothermally crystallized at 121 °C for $t=0$, $t=50$, $t=125$, and $t=200$. Both rows are characteristics of typical spinodal decomposition phase separation. Figure 4(a1) shows that the interface between two phases is not clear when the second temperature quench occurs. This means LLPS at 130 °C is not yet complete and the system remains in the early stage of phase separation for the upper image. In contrast, the clear interface between the two phases visible in Fig. 4(a2) illustrates that LLPS at 130 °C is almost complete. Therefore, the second quench occurs in the later stage of LLPS for the lower row of image.

Figures 5–7 show time evolution of the crystal order parameter with three different initial concentrations. In each figure, the time evolution of the orientational order parameter is shown; the upper and lower rows represent different quench times (t^*). From Fig. 3, we know that the second temperature quench happens in the early stage of phase separation for upper row images (a1)–(d1), while it happens in the late stage of phase separation for lower row images (a2)–(d2). In these three figures, the number density of spherulites is obviously lower and spherulite sizes are smaller when the first quench continues for a longer period of time which are shown in the lower row image either in Fig. 5 (after $t=200$) or in Figs. 6 and 7 (after $t=100$). In contrast to Figs. 4(a1)–4(d1), we see that the crystal nuclei are formed at the interface of the phase-separated domains in Figs. 6(a1)–(d1), which implies that at high crystallization temperatures, in-

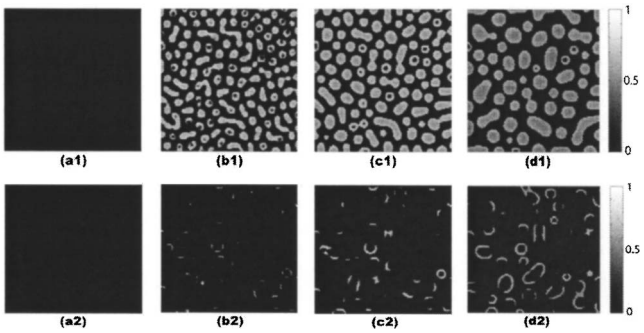

FIG. 5. Time evolution of the crystal order parameter (ψ) with PEH/PEB=35/65 and two different quench times (t^*) for upper row images (a1)–(d1) and lower row images (a2)–(d2). (a1) LLPS at 130 °C for $t=25$, then isothermally crystallized at 121 °C for $t=0$, (b1) $t=25$, (c1) $t=75$, and (d1) $t=175$. (a2) LLPS at 130 °C for $t=100$, then crystallized at 121 °C for $t=0$, (b2) $t=50$, (c2) $t=100$, and (d2) $t=200$.

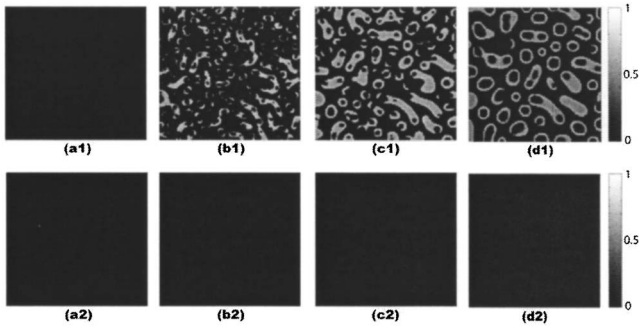

FIG. 6. Time evolution of crystal order parameter (ψ) with the PEH/PEB =40/60 and two different quench time (t^*) for upper row images (a1)–(d1) and lower row images (a2)–(d2). (a1) LLPS at 130 °C for t=25, then isothermally crystallized at 121 °C for t=0, (b1) t=25, (c1) t=75, and (d1) t =175. (a2) LLPS at 130 °C for t=100, then isothermally crystallized at 121 °C for t=0, (b2) t=50, (c2) t=125 and (d2) t=200.

creased nucleation might not occur without the influence of the interface formed through spinodal LLPS. Here the interface of LLPS can be defined by the absolute magnitude of the gradient ($|\nabla\phi|$) since the peak of $|\nabla\phi|$ is reached at the interface. It is further noted from Figs. 5–7 that crystals are growing toward the PEH rich domains, which is probably due to the lack of PEH chains in the PEB rich domains. This is also consistent with the experimental results of Zhang *et al.*[31,32]

Figure 8 shows time evolution of compositional order parameter with the PEH/PEB=45/55. The simulated system was first kept at 140 °C undergoing LLPS for a very long time (t=600) and then deeply quenched to room temperature (25 °C). It is clear that small secondary domains of each polymer appear in the larger primary domains which are formed during LLPS by the first temperature quench. This is because after the second quench the initially favored length scale (the fastest growing fluctuation), which can be determined from linearized theory, is much smaller than the primary structural scale. In other words, if the second temperature-quench depth is only slightly deeper than the first, no secondary structure is observed. Only a slight growth in the original structure results from continued domain broadening. As the simulation proceeds, these initially dynamically favorable secondary domains, creating large interfacial areas and a large increase in the surface free energy, will finally dissolve into the surrounding phases.

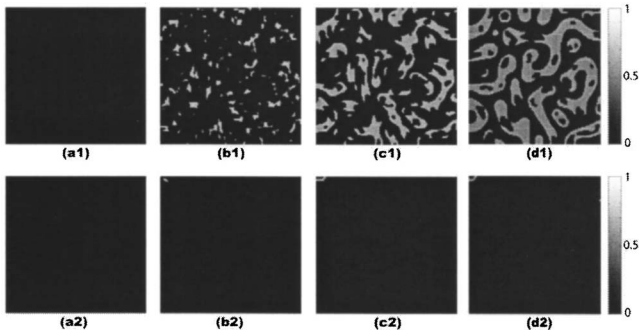

FIG. 7. Time evolution of crystal order parameter (ψ) with the PEH/PEB =45/55 and two different quench times (t^*) for upper row images (a1)–(d1) and lower row images (a2)–(d2). (a1) LLPS at 130 °C for t=25, then isothermally crystallized at 121 °C for t=0, (b1) t=25, (c1) t=75, and (d1) t =175. (a2) LLPS at 130 °C for t=100, then isothermally crystallized at 121 °C for t=0, (b2) t=50, (c2) t=125, and (d2) t=200.

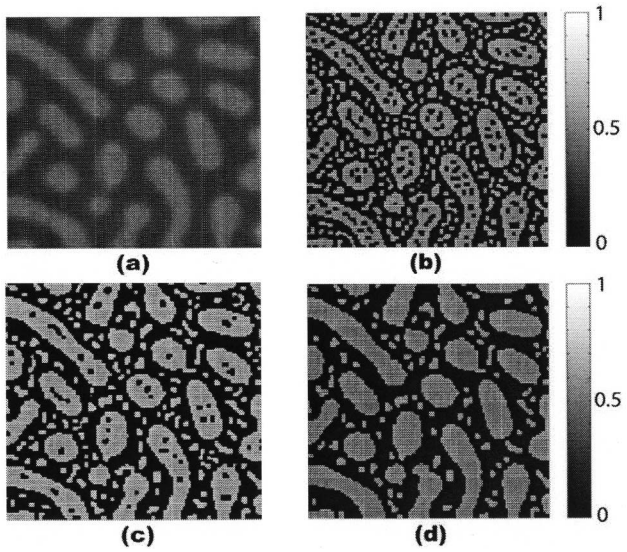

FIG. 8. Time evolution of compositional order parameter (ϕ) with the PEH/PEB=45/55. (a) LLPS at 140 °C for t=600, then quenched to 25 °C for t=0, (b) t=5, (c) t=15, and (d) t=300.

Figure 9 shows time evolution of crystal order parameter with the PEH/PEB=45/55. When the system is quenched to about room temperature, continuous crystallization occurs in the PEH-rich region of both of the original PEH-rich and PEB-rich domains. Compared to the time evolution of compositional order parameter shown in Fig. 8, it is clear that most of the nuclei found are located at the interface of the phase-separated domains. This can be explained as follows. Although the second temperature-quench time corresponds to the late stage of phase separation, the equilibrium composition of one or two phases (PEH-rich or PEB-rich domains) will be in the unstable spinodal region for very deep quench. Therefore, the intrinsic physical mechanism is the same as former cases shown in the upper row image of Figs. 5–7.

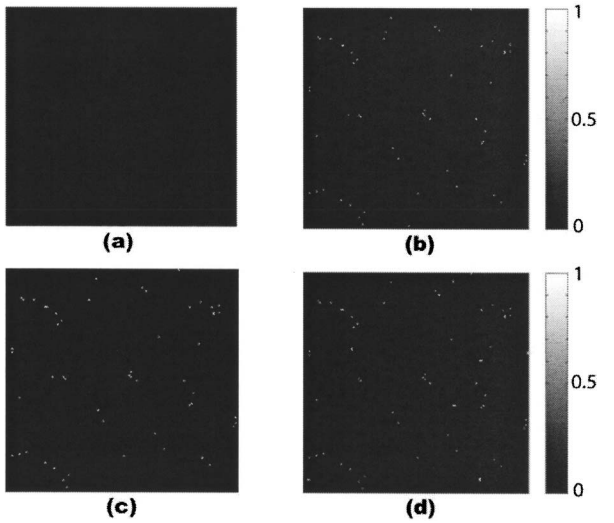

FIG. 9. Time evolution of crystal order parameter (ψ) with the PEH/PEB =45/55. (a) LLPS at 140 °C for t=600, then isothermally crystallized at 25 °C for t=0, (b) t=5, (c) t=15, and (d) t=300.

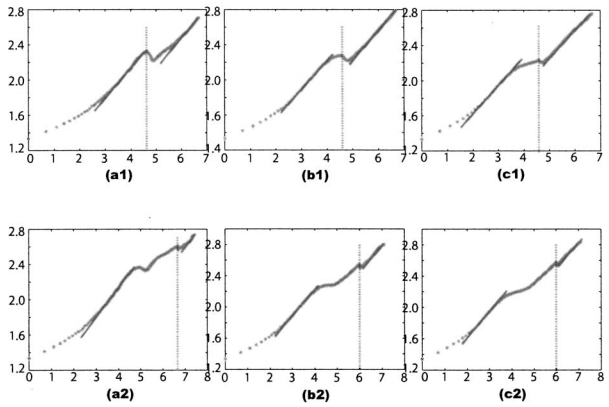

FIG. 10. Log-log plot of the growth for the averaged length scale in the pattern formation of phase separation. The slope of the thick line is 1/3 and the second temperature-quench time is recorded by the dash dot line. The initial concentration (ϕ_0) and the second temperature-quench time (t^*) are (a1) $\phi_0=0.35$, $t^*=25$, (a2) $\phi_0=0.35$, $t^*=200$, (b1) $\phi_0=0.4$, $t^*=25$, (b2) $\phi_0=0.4$, $t^*=100$, (c1) $\phi_0=0.45$, $t^*=25$, and (c2) $\phi_0=0.45$, and $t^*=100$.

Figure 10 shows time evolution of the averaged scattering wave number corresponding to the growth of length scale for the compositional order parameter (ϕ). The simulated system with three initial concentrations first undergoing LLPS at 130 °C for different times is then quenched to 121 °C for crystallization. The growth of domain size $L(t)$ is related to the averaged scattering wave number $q(t)$ as

$$L(t) = \frac{2\pi}{\langle q(t)\rangle},$$

where

$$\langle q(t)\rangle = \frac{\Sigma_q q S(q,t)}{\Sigma_q S(q,t)}.$$

Here q is the modulus of the wave vector $q=(2\pi/N)\times(m_1,m_2)$ with m_1, m_2 integers, and N the system size. The spherically averaged structure function $S(q,t)$ is defined by

$$S(q,t) = \frac{\Sigma_{\hat{q}} S(\mathbf{q},t)}{\Sigma_{\hat{q}} 1},$$

where $\hat{\boldsymbol{q}}$ indicates the set of wave vectors contained in a spherical shell and $S(\boldsymbol{q},t)$ is the scattering function, which is the Fourier transform of the correlation function. It is well established that the growth of domain size $L(t)$ in binary mixture for phase separation without hydrodynamics satisfies the scaling law[48]

$$L(t) \propto t^{1/3}.$$

Figure 10 shows that our model satisfies the scaling hypothesis very well for the later stage of phase separation by the first temperature quench. This is quite reasonable since we are not yet considering the effects of hydrodynamics. The scaling law also holds after the second temperature quench. This can be explained as follows. Since the second quench is slightly deeper than the first one, as shown in Fig. 10, only a slight growth in the original structure and continued domain coarsening will take place. The pattern formation after the second quench is stilled controlled by further diffusion and coarsening which is reflected by the second slope indicating the same scaling exponent.[49] In addition, it should be mentioned that the averaged domain size will become smaller right after the second temperature quench shown in Fig. 10. This is because the favored length scale after the second quench is smaller compared to the primary structural scale formed by the first quench and it will cause the decrease in the averaged domain size.

V. CONCLUSION

We propose a phenomenological model to describe the kinetic coupling of phase separation and crystallization in polymer blend systems. Our model can reproduce the phenomena observed in recent experiments.[29–33] Further, it captures some of the physical mechanisms for dynamics, such as the classical scaling hypothesis. As it is known that Landau free energy approach serves as a basis for studying phase separation and crystallization phenomena, we used this form for the total free energy when considering their coupling. We have constructed a coupling term that is consistent with Landau-type free energy and have found that it gives reasonable descriptions of the experiments. Our simple model to some extent reproduces all experimental results such as the decrease in number and size of crystallized spherulites with increasing time in phase separation, the preponderance of nuclei near the domain interface, and the subphase separation and subcrystallization occurring when the second quench is very deep. Our work is a first step in revealing the mechanism underlying the kinetic interaction between phase separation and crystallization. More detailed models regarding the microscopic crystal structures should be studied in the future.[12,21,50,51]

ACKNOWLEDGMENTS

We are grateful to Dr. Xiaohua Zhang and Professor Charles C. Han for their valuable discussions; Dr. Sharon Murrel for the help on the English writing. Pingwen Zhang is partially supported by the National Science Foundation of China under Grant No. 20490222 and the special funds for Major State Research Projects (2005CB321704).

[1] D. R. Paul and S. Newmann, *Polymer Blends* (Academic, New York, 1978), Vols. I and II.
[2] O. Olabish, L. M. Robeson, and M. T. Shaw, *Polymer-Polymer Miscibility* (Academic, New York, 1979).
[3] K. Solc, *Polymer Compatibility and Incompatibility* (Harwood Academic, New York, 1980).
[4] T. Kyu and H. W. Chiu, Phys. Rev. E **53**, 3618 (1996).
[5] H. W. Chiu and T. Kyu, J. Chem. Phys. **103**, 7471 (1995).
[6] H. W. Chiu and T. Kyu, J. Chem. Phys. **108**, 3249 (1998).
[7] N. P. Balsara, L. J. Fetters, N. Hadjichristidis, D. J. Lohse, C. C. Han, W. W. Graesslley, and R. Krishnamoorti, Macromolecules **25**, 6137 (1992).
[8] A. A. Lefebvre, J. H. Lee, N. P. Balsara, and B. Hammouda, J. Chem. Phys. **116**, 4777 (2002).
[9] K. Sasaki and T. Hashimoto, Macromolecules **17**, 2818 (1984).
[10] T. Izumitani and T. Hashimoto, J. Chem. Phys. **83**, 3694 (1985).
[11] C. Y. Chen, W. M. Yunus, H. W. Chiu, and T. Kyu, Polymer **38**, 4433 (1997).
[12] R. Mehta and T. Kyu, J. Polym. Sci., Part B: Polym. Phys. **42**, 2892 (2004).
[13] J. D. Hoffman and R. L. Miller, Macromolecules **21**, 3038 (1988).
[14] M. Okada, M. Nishi, M. Takahashi, H. Matsuda, A. Toda, and M. Hikodaka, Polymer **39**, 4535 (1998).

[15] K. Kaji, K. Nishida, G. Matsuba, T. Kanaya, and M. Imai, J. Macromol. Sci., Phys. **B42**, 709 (2003).
[16] G. Matsuba, K. Kaji, T. Kanaya, and K. Nishida, Phys. Rev. E **65**, 061801 (2002).
[17] M. Imai, K. Kaji, and T. Kanaya, Macromolecules **27**, 7103 (1994).
[18] M. Imai, K. Kaji, and T. Kanaya, Phys. Rev. Lett. **71**, 4162 (1993).
[19] C.-M. Chen and P. G. Higgs, J. Chem. Phys. **108**, 4305 (1998).
[20] A. A. Wheeler, W. J. Boettinger, and G. B. McFadden, Phys. Rev. A **45**, 7424 (1992).
[21] T. Kyu, H.-W. Chiu, A. J. Guenthner, Y. Okabe, H. Saito, and T. Inoue, Phys. Rev. Lett. **83**, 2749 (1999).
[22] H. Wang, K. Shimizu, H. Kim, E. K. Hobbie, Z. G. Wang, and C. C. Han, J. Chem. Phys. **116**, 7311 (2002).
[23] G. Matsuba, K. Shimizu, H. Wang, Z. G. Wang, and C. C. Han, Polymer **45**, 5137 (2004).
[24] K. Shimizu, H. Wang, Z. G. Wang, G. Matsuba, H. Kim, and C. C. Han, Polymer **45**, 7061 (2004).
[25] H. Tanaka and T. Nishi, Phys. Rev. A **39**, 783 (1989).
[26] N. Inaba, K. Sato, S. Suzuki, and T. Hashimoto, Macromolecules **19**, 1690 (1986).
[27] P. D. Olmsted, W. C. K. Poon, T. C. B. Mcleish, N. J. Terrill, and A. J. Ryan, Phys. Rev. Lett. **81**, 373 (1998).
[28] N. Inaba, T. Yamada, S. Suzuki, and T. Hashimoto, Macromolecules **21**, 407 (1988).
[29] H. Wang, K. Shimizu, E. K. Hobbie, Z. G. Wang, J. C. Meredith, A. Karim, E. J. Amis, B. S. Hsiao, E. T. Hsieh, and C. C. Han, Macromolecules **35**, 1072 (2002).
[30] G. Matsuba, K. Shimizu, H. Wang, Z. G. Wang, and C. C. Han, Polymer **44**, 7459 (2003).
[31] X. H. Zhang, Z. G. Wang, M. Muthukumar, and C. C. Han, Macromol. Rapid Commun. **26**, 1285 (2005).
[32] X. H. Zhang, Z. G. Wang, X. Dong, D. J. Wang, and C. C. Han, J. Chem. Phys. **125**, 024907 (2006).
[33] X. H. Zhang, Z. G. Wang, R. Y. Zhang, and C. C. Han, Macromolecules **39**, 9285 (2006).
[34] P. M. Chaikin and T. C. Lubensky, *Principles of Condensed Matter Physics* (Cambridge University Press, New York, 1995).
[35] J. R. Dorgan, J. Chem. Phys. **98**, 9094 (1993).
[36] K. R. Elder, F. Drolet, J. M. Kosterlitz, and M. Grant, Phys. Rev. Lett. **72**, 677 (1994).
[37] J. I. Lauritzen and J. D. Hoffman, J. Chem. Phys. **31**, 1680 (1959).
[38] J. I. Lauritzen and J. D. Hoffman, J. Res. Natl. Bur. Stand., Sect. A **64A**, 73 (1960).
[39] *Treatise on Solid State Chemistry*, edited by N. B. Hannay (Plenum, New York, 1976).
[40] J. D. Gunton, M. San Miguel, and P. S. Sahni, *Phase Transitions and Critical Phenomena* (Academic, New York, 1983).
[41] A. Matsuyama, J. Phys. Soc. Jpn. **75**, 084602 (2006).
[42] A. Matsuyama, J. Phys. Soc. Jpn. **75**, 034604 (2006).
[43] R. A. Matkar and T. Kyu, J. Chem. Phys. **110**, 12728 (2006).
[44] R. A. Matkar and T. Kyu, J. Chem. Phys. **110**, 16059 (2006).
[45] G. Matsuba, T. Kanaya, M. Saito, K. Kaji, and K. Nishida, Phys. Rev. E **62**, R1497 (2000).
[46] T. Kyu, R. Mehta, and H. W. Chiu, Phys. Rev. E **61**, 4161 (2000).
[47] H. Xu, R. A. Matkar, and T. Kyu, Phys. Rev. E **72**, 011804 (2005).
[48] A. J. Bray, Adv. Phys. **43**, 357 (1994).
[49] J. B. Collins, A. Chakrabarti, and J. D. Gunton, Phys. Rev. B **39**, 1506 (1989).
[50] R. Mehta, W. Keawwattana, A. L. Guenthner, and T. Kyu, Phys. Rev. E **69**, 061802 (2004).
[51] D. Nwabunma and T. Kyu Ed, *Polyolefin Blends* (Wiley, New York, 2007).